Dalton Transactions

ROYAL SOCIETY OF CHEMISTRY

PAPER

View Article Online
View Journal | View Issue

Cite this: *Dalton Trans.*, 2024, **53**, 2275

Unravelling the 6sp ← 6s absorption spectra of Bi(III) complexes†

Charlene Harriswangler, Fátima Lucio-Martínez, Aurora Rodríguez-Rodríguez, David Esteban-Gómez and Carlos Platas-Iglesias *

Received 9th November 2023,
Accepted 20th December 2023

DOI: 10.1039/d3dt03744d

rsc.li/dalton

We report a spectroscopic and computational study that investigates the absorption spectra of Bi(III) complexes, which often show an absorption band in the UV region (~270–350 nm) due to 6sp ← 6s transitions. We investigated the spectra of three simple complexes, $[BiCl_5]^{2-}$, $[BiCl_6]^{3-}$ and $[Bi(DMSO)_8]^{3+}$, which show absorption maxima at 334, 326 and 279 nm due to $^3P_1 \leftarrow {}^1S_0$ transitions. Theoretical calculations based on quasi-degenerate N-electron valence perturbation theory to second order (QD-NEVPT2) provide an accurate description of the absorption spectra when employing CAS(2,9) wave functions. We next investigated the absorption spectra of the [Bi(NOTA)] complex (H_3NOTA = 1,4,7-triazacyclononane-1,4,7-triacetic acid), which forms ternary complexes $[Bi(NOTA)X]^-$ (X = Cl, Br or I) in the presence of excess halide in aqueous solutions. Halide binding has an important impact on the position of the $^3P_1 \leftarrow {}^1S_0$ transition, which shifts progressively to longer wavelengths from 282 nm ([Bi(NOTA)]) to 298 nm (X = Cl), 305 nm (X = Br) and 325 nm (X = I). Subsequent QD-NEVPT2 calculations indicate that this effect is related to the progressive stabilization of the spin–orbit free states associated with the $6s^16p^1$ configuration on increasing the covalent character of the metal–ligand(s) bonds, rather than with significant differences in spin–orbit coupling (SOC). These studies provide valuable insight into the coordination chemistry of Bi(III), an ion with increasing interest in targeted alpha therapy due to the possible application of bismuth isotopes bismuth-212 (^{212}Bi, $t_{1/2}$ = 60.6 min) and bismuth-213 (^{213}Bi, $t_{1/2}$ = 45.6 min).

Introduction

The coordination chemistry of Bi(III) in aqueous solution is probably the least well-established among the heavy stable elements. The Bi(III) ion is considered as a borderline acid within Pearson's classification, and it is known to form stable complexes with polyaminocarboxylate ligands containing O and N donor atoms.[1] Bi(III) compounds were introduced as remedies for gastrointestinal disorders by the late 18th century,[2] and they are still in use (*i.e.* bismuth subsalicylate, marketed as Pepto-Bismol®). Simple bismuth salts have also been used to treat different microbial infections, including syphilis, colitis, diarrhoea and dermal wounds. More recently, Bi(III) coordination chemistry has experienced renewed interest due to the interesting decay properties of some of its radioisotopes. Indeed, both bismuth-212 (^{212}Bi, $t_{1/2}$ = 60.6 min) and bismuth-213 (^{213}Bi, $t_{1/2}$ = 45.6 min) have been highlighted as two of the most promising radioisotopes for application in targeted alpha therapy (TAT).[3–5] For this purpose, the radioisotope must be coordinated by a suitable ligand that ensures stable complexation and the specific irradiation of the tumour cells. Most preclinical studies have used DTPA (diethylenetriaminepentaacetic acid) derivatives for this purpose,[6] but other polyaminopolycarboxylate chelators are currently being developed for this application, as the complexes of acyclic ligands such as DTPA at times present lower stability compared with cyclic analogues such as DOTA (1,4,7,10-tetraazacyclododecane-1,4,7,10-tetraacetic acid).[7–14]

The Bi(III) ion has a $[Xe]4f^{14}5d^{10}6s^2$ electron configuration, shared as well with Pb(II) and Tl(I). The coordination chemistry of these metal ions is heavily impacted by the lone-pair effect,[12,15–18] which refers to the reluctance of the $6s^2$ electrons to be ionized or participate in chemical bonding. The $6s^2$ lone pair is often stereochemically active, which results in an uneven distribution of the donor atoms in the inner coordination sphere.[19] The absorption spectra of Bi(III) complexes often show a band in the UV region of the spectrum (~270–350 nm) that is attributed to a 6sp ← 6s transition. The absorption spectra of Pb(II) complexes show similar features, but the position of this band is generally shifted to higher

Universidade da Coruña, Centro de Interdisciplinar de Química e Bioloxía (CICA) and Departamento de Química, Facultade de Ciencias, 15071 A Coruña, Galicia, Spain. E-mail: carlos.platas.iglesias@udc.es

† Electronic supplementary information (ESI) available: Spectroscopic characterization of the ligands and their precursors, spectrophotometric experiments and structural details of the geometries obtained with DFT. See DOI: https://doi.org/10.1039/d3dt03744d

energies (*ca.* 210–260 nm).[20] A correlation between the position of this band and the stereochemical activity of the $6s^2$ lone-pair was proposed for Pb(II).[20]

Theoretical calculations were used to analyse the absorption spectra of Bi(III) complexes, specifically based on time-dependent density functional theory (TDDFT). These studies confirmed the 6sp ← 6s character of the absorption band around 300 nm. The presence of Cl^-, Br^- and I^- anions in the first coordination sphere shifts the main absorption band to lower energies, an effect that is enhanced as the halide anion becomes heavier.[16,21] However, the results obtained with TDDFT calculations are highly dependent on the functional used, in particular on the amount of Hartree-Fock (HF) exchange. Furthermore, spin–orbit coupling (SOC) effects, which may be important for heavy atoms like Bi, were not considered so far. The limitations of TDDFT-SOC calculations for the calculation of excited states of heavy atoms have also been recently pointed out, as the perturbative SOC coupling treatment is not appropriate if its magnitude is comparable to the excited state energy gap.[22]

In this work, we sought to investigate the absorption spectra of a series of small Bi(III) complexes (Scheme 1), using both TDDFT calculations and wave function approaches. Thus, we investigated the octahedral $[BiCl_6]^{3-}$ complex as a model system, and compared its absorption spectrum with that of the square pyramidal $[BiCl_5]^{2-}$ complex. The structure of the dimethylsulfoxide (DMSO) solvate $[Bi(DMSO)_8]^{3+}$ was established using EXAFS, large-angle X-ray scattering, and crystallographic studies, which evidenced the formation of an eight-coordinated structure.[23] Herein, we investigated the absorption spectra of this simple complex and analyzed the performance of TDDFT and calculations based on the complete active space self-consistent field (CASSCF) approach. Given the importance of Bi(III) complexes with polyaminopolycarboxylate ligands, we chose [Bi(NOTA)] as a model complex (H_3NOTA = 2,2′,2″-(1,4,7-triazacyclononane-1,4,7-triyl)triacetic acid). This simple complex was scarcely investigated, though kinetic studies demonstrated slow dissociation in 1 M $HClO_4$.[24] Bifunctional derivatives were also tested as Bi(III)-based radiopharmaceuticals.[25,26] This compound is coordinatively unsaturated and binds halide anions to form ternary complexes [Bi(NOTA)X]$^-$ (X = Cl, Br or I). We show that anion binding has an important impact on the absorption spectra of the complex. This, along with the absence of chromophores in the ligand, is what makes it attractive for this computational study, which can be extended to more complex systems later on.

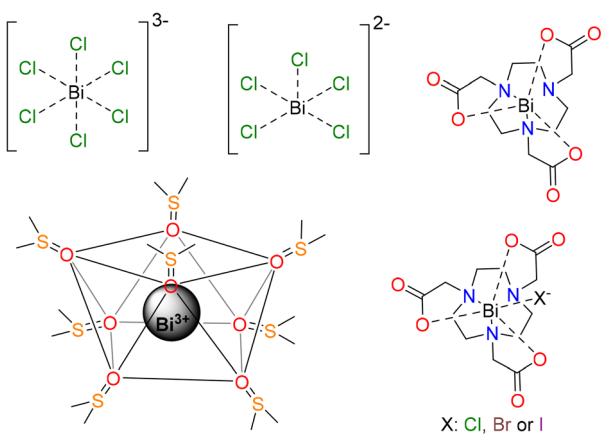

Scheme 1 Bi(III) complexes investigated in this work.

Results and discussion

Calculations on the free Bi(III) ion

The absorption spectra of Bi(III) complexes are characterised by the presence of a rather intense absorption arising from excitation from the $^1S_0$ ground state level of the $6s^2$ configuration to the excited state levels of the $6s^16p^1$ configuration. These are the $^3P_0$, $^3P_1$, $^3P_2$ and $^1P_1$ levels, which for the free Bi(III) ion have the energies shown in Table 1.[27] Early computational work revealed that the theoretical treatment of the Bi(III) ion is far from being straightforward, due to the importance of both relativistic and electron correlation effects.[28] Herein, initial tests were performed to assess the performance of TDDFT in comparison with NEVPT2 (N-electron valence perturbation theory to second order), which is a multireference method that incorporates electron correlation to the CASSCF wave function through perturbation theory. TDDFT calculations were carried out with the pure PBE functional and its hybrid version PBE0 (25% HF exchange). The pure TPSS functional was also tested, as it has been previously used for TDDFT calculations of Bi(III) complexes.[16] The results of these calculations are summarised in Table 1.

TDDFT calculations were performed incorporating SOC effects, using the effective potential and mean-field approaches (SOMF(1X)). The results shown in Table 1 indicate that the functionals tested in this study provide energies of the levels associated with the $6s^16p^1$ configuration that deviate significantly from the experimental data. The pure PBE functional gives better results than the hybrid counterpart PBE0, while the TPPS functional yields slightly worse results than PBE. The differences between experimental and calculated energies obtained with PBE are high, in particular for the $^3P_0$ level. For

Table 1 Energies (cm^{-1}) of the levels arising from the $6s^16p^1$ configuration of the Bi(III) free ion with respect to the ground $^1S_0$ level.[a]

	$^3P_0$	$^3P_1$	$^3P_2$	$^1P_1$
PBE0	59 178	66 070	100 180	117 158
PBE	62 576	69 311	103 220	113 098
TPSS	61 605	68 396	102 740	118 567
CASSCF	67 439	72 153	87 625	119 111
NEVPT2	70 938	75 899	96 385	114 558
QD-NEVPT2	76 124	79 894	96 310	113 461
Exp./cm^{-1}	75 539	79 283	95 726	112 602
Exp./nm	132.4	126.1	104.4	88.8

[a] Experimental data from ref. 27.

this level, a deviation of ~13 000 cm^{-1} is obtained, which represents *ca.* 17%. While the purpose of this work is not to establish a benchmark for DFT methods, our results indicate that the prediction of the absorption spectra of Bi(III) compounds using DFT may be problematic.

We next explored the performance of the CASSCF method, using an active space that included the two $6s^2$ electrons distributed over the 6s and 6p orbitals CAS(2,4). The CASSCF method gives more accurate energies of the levels associated with the $6s^16p^1$ configuration than any of the DFT methods. Incorporating electron correlation using NEVPT2 significantly improves the quality of the calculated results, which deviate <650–4600 cm^{-1} from the experimental data. In NEVPT2, SO effects are incorporated using quasi-degenerate perturbation theory, where the NEVPT2 corrections are included as improved diagonal energies, but do not alter the composition of the reference state. This limitation can be overcome by using quasi-degenerate NEVPT2 (QD-NEVPT2), in which remixing of the reference states is allowed. The use of QD-NEVPT2 results in a dramatic improvement of the agreement between experimental and calculated energies, with deviations <900 cm^{-1}. Thus, we subsequently used QD-NEVPT2 to analyse the absorption spectra of Bi(III) complexes, unless otherwise indicated.

Absorption spectra of the $[BiCl_5]^{2-}$, $[BiCl_6]^{3-}$ and $[Bi(DMSO)_8]^{3+}$ complexes

The absorption spectra of the octahedral $[BiCl_6]^{3-}$ complex were investigated previously in non-aqueous solvents.[21,29,30] In aqueous media, both the $[BiCl_5]^{2-}$ and $[BiCl_6]^{3-}$ species are present in solution at HCl concentrations higher than 2 M and room temperature, as demonstrated by EXAFS measurements.[31] A spectrophotometric study concluded that under these conditions, the square pyramidal $[BiCl_5]^{2-}$ complex is the main species present in solution, which is characterised by an absorption maximum at 327 nm.[32] The absorption spectrum of a solution of $BiCl_3$ (5×10^{-5} M) in 2 M HCl (Fig. 1) displays maxima at 327 nm and 231 nm, as well as an additional band at 260 nm. This feature is not observed in the spectrum of $[BiCl_6]^{3-}$ obtained in acetonitrile solution, which shows maxima at 334 and 231 nm, in agreement with the literature data.[21] This suggests that the $[BiCl_5]^{2-}$ complex is indeed the main species present in solution.

The geometry of $[BiCl_6]^{3-}$ optimized using DFT (see the computational details below) displays octahedral symmetry with Bi–Cl distances of 2.751 Å. For $[BiCl_5]^{2-}$, our DFT calculations afford a square-pyramidal geometry with a short axial Bi–Cl distance of 2.561 Å and Bi–Cl distances of 2.721 Å involving the basal plane. An EXAFS study provided an average Bi–Cl distance of 2.631 Å for a 2 M HCl solution of Bi(III) at 30 °C, with the fit of the data affording a coordination number of 5.3.[31] The stabilization of square-pyramidal coordination over a trigonal bipyramidal geometry is likely the result of the stereochemical activity of the Bi(III) $6s^2$ lone pair. Indeed, square pyramidal coordination was predicted by computational studies performed on the isoelectronic $[PoCl_5]^-$.[33,34]

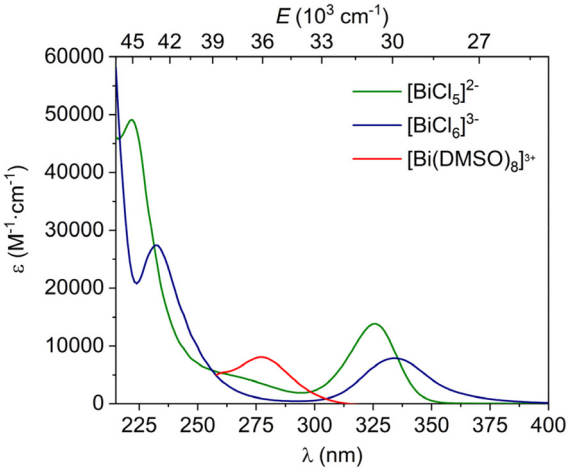

Fig. 1 Absorption spectra of a solution of $BiCl_3$ (5×10^{-5} M) in 2 M HCl, where the $[BiCl_5]^{2-}$ complex is the main species in solution (green trace); a solution of $BiCl_3$ (5×10^{-5} M) in acetonitrile in the presence of 45 equiv. of $(nBu)_4NCl$, where the main species in solution is the octahedral $[BiCl_6]^{3-}$ complex (blue trace); and a 5×10^{-5} M solution of $[Bi(DMSO)_8]^{3+}$ (red trace).

Furthermore, the $6s^2$ lone pair in $[BiCl_5]^{2-}$ is polarised by a small but significant p character (2.0% according to natural bond orbital analysis), while in $[BiCl_6]^{3-}$, the lone pair has 100% 6s character, according to natural bond orbital (NBO) analysis. Studies performed on the Po(IV) analogue evidenced that a better match of the absorption spectral data was found with a model where the complex holds a water molecule ($[PoCl_5(H_2O)]^-$).[34] However, calculations performed on the $[BiCl_5(H_2O)]^{2-}$ system (using an implicit PCM solvation model) resulted in the expulsion of the water molecule from the inner-coordination sphere, with a calculated Bi···O distance of 2.754 Å. Thus, the lower oxidation state of the metal ion in the Bi(III) complex results in a weak interaction with the water ligand.

The absorption spectra of the $[BiCl_5]^{2-}$ and $[BiCl_6]^{3-}$ species were subsequently analysed using QD-NEVPT2 calculations based on a CAS(2,4) active space (two electrons distributed over the orbitals with main 6s and 6p character). These calculations predicted the lowest energy absorption of $[BiCl_5]^{2-}$ and $[BiCl_6]^{3-}$ at 286 and 267 nm, respectively, in sharp contrast to the experimental values of 327 and 334 nm. However, a dramatic improvement of the results was obtained when incorporating five additional (virtual) orbitals with significant 6s and 6p character into the active space, as demonstrated by Löwdin[35] population analysis (Fig. 2). This provides a more balanced description of covalent interactions in the system, by incorporating additional antibonding orbitals into the active space.[36] Besides, the wave function becomes more flexible, providing a more accurate treatment of electron correlation.[37] In the case of transition metal complexes, this is generally achieved by incorporating a second shell of metal-based d orbitals into the active space.[38] The lack of proper description of covalent interactions in $[BiCl_5]^{2-}$ and $[BiCl_6]^{3-}$ results in a

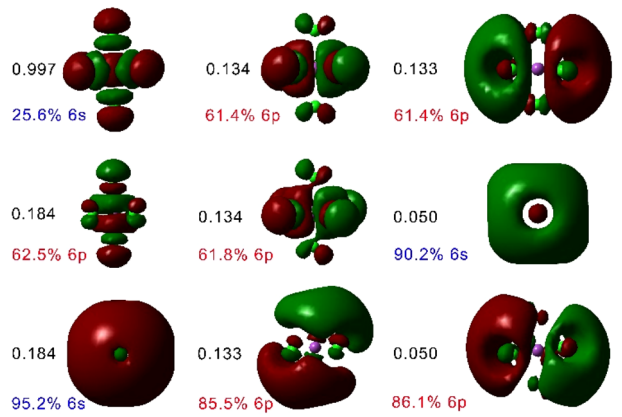

Fig. 2 Active space orbitals used for QD-NEVPT2 calculations based on a CAS(2,9) active space for $[BiCl_6]^{3-}$, plotted using an isodensity surface of 0.01 a. u., their occupation numbers and the contributions from Bi(III) 6s and 6p orbitals obtained with Löwdin population analysis.

clear overestimation of transition energies by QD-NEVPT2 calculations based on CAS(2,4) wave functions. Eight out of the nine orbitals included in the active space for $[BiCl_6]^{3-}$ have dominant Bi character (>60%, Fig. 2), though significant contributions from Cl orbitals can be noticed. The ninth orbital, which has the largest occupation in the state-average wave function, contains ~26% contribution of the Bi 6s orbital, and shows antibonding character with respect to the Bi–Cl interaction.

The QD-NEVPT2 calculations based on CAS(2,9) wave functions predicted two absorption maxima at 315 and 215 nm for the $[BiCl_6]^{3-}$ complex, assigned to the $^3P_1 \leftarrow {}^1S_0$ (or $^3T_{1u} \leftarrow {}^1A_{1g}$ in O_h symmetry) and $^1P_1 \leftarrow {}^1S_0$ ($^1T_{1u} \leftarrow {}^1A_{1g}$ in O_h symmetry) transitions, respectively. The $^1P_1$ and $^3P_1$ states can mix orbitally, and thus the $^3P_1 \leftarrow {}^1S_0$ and $^1P_1 \leftarrow {}^1S_0$ transitions are both spin–orbit and electric dipole allowed, resulting in sizeable oscillator strengths f_{osc} (Table 2). In contrast, the $^3P_0 \leftarrow {}^1S_0$ and $^3P_2 \leftarrow {}^1S_0$ transitions are forbidden, resulting in f_{osc} values of zero. The calculated oscillator strengths follow the trend of experimental extinction coefficients well (Table 2).

The spectral data calculated for $[BiCl_5]^{2-}$ with QD-NEVPT2 also show good agreement with the experimental spectrum. The excited free-ion $^3P_1$ level splits into two states (^3E and $^3A_1$) in the C_{4v} symmetry, which results in two transitions ($^3E \leftarrow {}^1A_1$ and $^3A_1 \leftarrow {}^1A_1$) at slightly different calculated wavelengths of 325 and 315 nm, in good agreement with the experimental absorption at 326 nm. These two transitions display significant f_{osc} values, as they are both spin–orbit and electric dipole allowed. A similar situation holds for the $^1P_1$ state, which leads to two transitions at 236 ($^1A_1 \leftarrow {}^1A_1$) and 207 nm ($^1E \leftarrow {}^1A_1$), in good agreement with the experimental value (222 nm). Our calculations provide a third absorption with a high value of f_{osc} of 83.1×10^{-3}, which can be attributed to the $^3E(^3P_2) \leftarrow {}^1A_1$ transition. Inspection of the composition of the SOC states shows that the sizeable intensity of the latter transition is related to the mixing of the $^3E(^3P_2)$ and $^3E(^3P_1)$ states, a situation that is not possible for the O_h point group due to the different symmetries of the states arising from the $^3P_2$ and $^3P_1$ free-ion levels. Thus, the additional feature observed at 257 nm in the absorption spectrum recorded in 2 M HCl is consistent with $[BiCl_5]^{2-}$ being the major species present in solution.

The Bi(III) solvates in DMSO were investigated using EXAFS and large-angle X-ray scattering. These studies indicated that the Bi(III) ion is eight-coordinated in solution with Bi–O distances of 2.41 Å.[23] Our DFT calculations provided an optimized structure with approximate C_2 symmetry and Bi–O distances in the range of 2.440–2.512 Å (2.390–2.469 Å in the X-ray structure). The absorption spectrum of the $[Bi(DMSO)_8]^{3+}$ complex (5×10^{-5} M) displays a maximum at 279 nm that can be attributed to 6sp ← 6s excitation (Fig. 1). Subsequent QD-NEVPT2 calculations were thus carried out to get a more detailed analysis of the absorption spectrum. CAS(2,4) calculations did not provide virtual orbitals with significant Bi 6s and 6p character close to the active space, and thus QD-NEVPT2 calculations were performed based on the CAS (2,4) wave function. Our calculations predict three absorptions involving the SOC states arising from the $^3P_1$ free-ion term at 260.2 ($f_{osc} = 97.3 \times 10^{-3}$), 259.6 ($f_{osc} = 101.2 \times 10^{-3}$) and 258.2 ($f_{osc} = 130.6 \times 10^{-3}$), in good agreement with the experimental absorption maximum of 279 nm. Furthermore, up to nine of

Table 2 Wavelengths (nm), energies (cm^{-1}) of the levels arising from the $6s^16p^1$ configuration of $[BiCl_5]^{2-}$ and $[BiCl_6]^{3-}$ with respect to the ground $^1S_0$ level and oscillator strengths (f_{osc}).[a]

$[BiCl_6]^{3-}$ (O_h)	$^3P_0$ ($^3A_{1u}$)	$^3P_1$ ($^3T_{1u}$)	$^3P_2$ ($^3T_{2u} + {}^3E_u$)	$^1P_1$ ($^1T_{1u}$)
λ (nm)	324.7	315.0(×3)	225.6(×5)	215.0(×3)
λ_{exp}[b] (nm)	—	334	—	231
Energy (cm^{-1})	30 797	31 746	44 324	46 504
$10^3 \times f_{osc}$	0.0	179.1	0.0	869.6
ε[a]/M^{-1} cm^{-1}	—	9520	—	28 600
$[BiCl_5]^{2-}$ (C_{4v})	$^3P_0$ ($^3A_2$)	$^3P_1$ ($^3E + {}^3A_1$)	$^3P_2$ ($B_1 + {}^3E + {}^3A_2 + {}^3B_2$)	$^1P_1$ ($^1A_1 + {}^1E$)
λ (nm)	333.4	326.2(×2)/315.4	243.7/238.6 (×2)/218.5 (×2)	236.2/206.8(×2)
λ_{exp} (nm)	—	326	257	222
Energy (cm^{-1})	29 998	30 656/31 707	41 036/41 908/45 770	42 343/48 356
$10^3 \times f_{osc}$	0.0	55.2/54.2	0.0/83.1/0.0	74.2/532.6
ε/M^{-1} cm^{-1}	—			

[a] Calculated data obtained with QD-NEVPT2 calculations using CAS(2,9) active spaces. [b] Data from ref. 21.

the twelve 6sp ← 6s absoptions have significant f_{osc} values in the range of 16×10^{-3} to 449×10^{-3}, which is a clear result of the low symmetry of the complex. The different wavelengths of the absorption maxima observed for $[BiCl_6]^{3-}$, $[BiCl_5]^{2-}$ and $[Bi(DMSO)_8]^{3+}$ evidence that the 6sp ← 6s transitions are rather sensitive to the metal coordination environment (Fig. 1).

The energies of the $^3P_0$ and $^3P_2$ levels can be used to estimate the SOC constant λ using eqn (1) and (2), which can be combined to give eqn (3).[34]

$$E(^3P_0) = E(^3P) - 2\lambda \quad (1)$$

$$E(^3P_2) = E(^3P) + \lambda \quad (2)$$

$$\lambda = (E(^3P_2) - E(^3P_0))/3 \quad (3)$$

Our calculations provide very similar λ values for $[BiCl_6]^{3-}$ (λ = 4500 cm^{-1}), $[BiCl_5]^{2-}$ (λ = 4425 cm^{-1}) and $[Bi(DMSO)_8]^{3+}$ (λ = 5100 cm^{-1}, Table 3). The same approach provides λ = 6729 cm^{-1} for the free Bi(III) ion, in line with the expected reduction in λ in metal complexes compared with the free ion due to covalency.[34] We also note that for these complexes, the $^3P_0$ and $^3P_1$ levels show very similar energies and that the lowest-energy absorption is due to the $^3P_1 \leftarrow {}^1S_0$ transition. Thus, the higher energy of the $^3P_1 \leftarrow {}^1S_0$ transition calculated for $[Bi(DMSO)_8]^{3+}$ (260 nm) compared with $[BiCl_6]^{3-}$ (315 nm) and $[BiCl_5]^{2-}$ (326 nm) is not related to significant differences in the values of λ. However, we notice very significant differences in the energies of the spin–orbit free states of these complexes (Table 3). Indeed, the energies of the levels arising from the ^3P and ^1P states calculated for $[Bi(DMSO)_8]^{3+}$ are clearly higher than those of $[BiCl_6]^{3-}$ and $[BiCl_5]^{2-}$. Conversely, much higher energies are obtained for the free Bi(III) ion. This reflects an important stabilization of the excited states of the 6sp configuration (^3P and ^1P) with respect to the ^1S ground state as a result of complex formation. This effect becomes more important as the covalent character of the Bi(III)–ligand bonds increases.

Table 3 QD-NEVPT2 energies of the spin–orbit free states arising from the $6s^16p^1$ configuration of free Bi(III) and Bi(III) complexes with respect to the ground ^1S level and SOC constants λ (cm^{-1}).[a]

	^3P	^1P	λ
Bi(III)	89 564	110 485	6729
$[BiCl_6]^{3-}$	39 851(×3)	43 047(×3)	4500
$[BiCl_5]^{2-}$	34 147/41 366(×2)	37 148/45 587(×2)	4425
$[Bi(DMSO)_8]^{3+}$	46 477/48 479/49 900	48 216/50 090/51 438	5100
[Bi(NOTA)]	41 316/45 126(×2)	45 900/48 777(×2)	3625
$[Bi(NOTA)Cl]^-$	42 063(×2)/43 552	43 554(×2)/48 830	4114
$[Bi(NOTA)Br]^-$	40 872(×2)/41 342	41 354/41 910(×2)	3715
$[Bi(NOTA)I]^-$	34 082/35 720(×2)	36 483(×2)/40 580	3762

[a] Average values are provided for pseudo-degenerate levels, with the number of levels provided within parentheses. All calculations performed using CAS(2,9) wave functions, except for $[Bi(DMSO)_8]^{3+}$ (CAS (2,4)).

Absorption spectra of [Bi(NOTA)] and $[Bi(NOTA)X]^-$ (X = Cl, Br or I) complexes

The ^1H NMR spectrum of [Bi(NOTA)] recorded in D_2O solution shows a singlet at 4.33 ppm due to the methylenic protons of the pendant arms and two multiplets at 3.88 and 3.60 ppm associated with the protons of the macrocyclic unit (Fig. S1, ESI†). This points to an effective C_{3v} symmetry of the complex in solution, which is confirmed by the three signals observed in the ^{13}C NMR spectrum (Fig. S2, ESI†).

The absorption spectrum of the [Bi(NOTA)] complex displays an absorption band with a maximum at 282 nm that can be assigned to 6sp ← 6s transitions (Fig. 3). Addition of large excesses of Cl^-, Br^- or I^-, as the corresponding potassium salts, induces significant changes in the absorption spectrum, with the maximum of the absorption band shifting to 298 (X = Cl^-), 305 (X = Br^-) and 325 nm (X = I^-). The titrations show well-defined isosbestic points that suggest the presence of a single equilibrium in solution according to the following equation:

$$[Bi(NOTA)] + X^- \rightleftarrows [Bi(NOTA)X]^- (X = Cl, Br \text{ or } I) \quad (4)$$

The absorption spectral data were subsequently fitted to a 1 : 1 binding model affording apparent association constants of K_{11} = 7.74(7) (X = Cl), 7.76(4) (X = Br) and 10.19(2) (X = I). These equilibrium constants point to a weak interaction of the [Bi(NOTA)] complex with the halide anions. However, they are slightly higher than those reported for [Bi(DO3A)],[16] likely as a result of the lower denticity of $NOTA^{3-}$ compared with $DO3A^{3-}$. The equilibrium constants follow the trend $Cl^- \sim Br^- < I^-$, as would be expected considering the β_6 values reported for the formation of $[BiX_6]^{3-}$ complexes.[39] The fits of the data afforded the spectra of the ternary $[Bi(NOTA)X]^-$ species, which are shown in Fig. 3. The absorption spectra evidence a progressive shift of the absorption maximum to longer wavelengths as halide size increases (Cl<Br<I).

DFT calculations on [Bi(NOTA)] and $[Bi(NOTA)X]^-$ (X = Cl, Br or I) complexes and stereochemical activity of the Bi(III) $6s^2$ lone pair

DFT calculations provide an optimised geometry for the [Bi(NOTA)] system with a slightly distorted C_3 symmetry and Bi–O and Bi–N distances of 2.378(4) and 2.481(1) Å, respectively (Table 4). The minimum energy conformation corresponds to the $\Lambda(\delta\delta\delta)$ [or $\Delta(\lambda\lambda\lambda)$] isomer,[40,41] with the free energy of the $\Delta(\delta\delta\delta)/\Lambda(\lambda\lambda\lambda)$ enantiomeric pair being 8.2 kJ mol^{-1} higher. This conformation was observed in the solid state for $NOTA^{3-}$ derivatives with trivalent metal ions such as Ga(III).[42,43] Complexes of Bi(III) with hexadentate ligands such as $EDTA^{4-}$ generally complete the metal coordination environment with water molecules or form coordination polymers with bridging carboxylate groups in the solid state.[1] However, the Bi–O distances involving water molecules or carboxylate groups of neighbouring complex entities are generally long (2.63–3.19 Å) compared to those within the $[Bi(EDTA)]^{2-}$ unit (2.28–2.60 Å). Optimizations performed on the $[Bi(NOTA)(H_2O)]$ system resulted in a structure where the water molecule is involved in hydrogen bonds with the carboxylate groups, rather than coor-

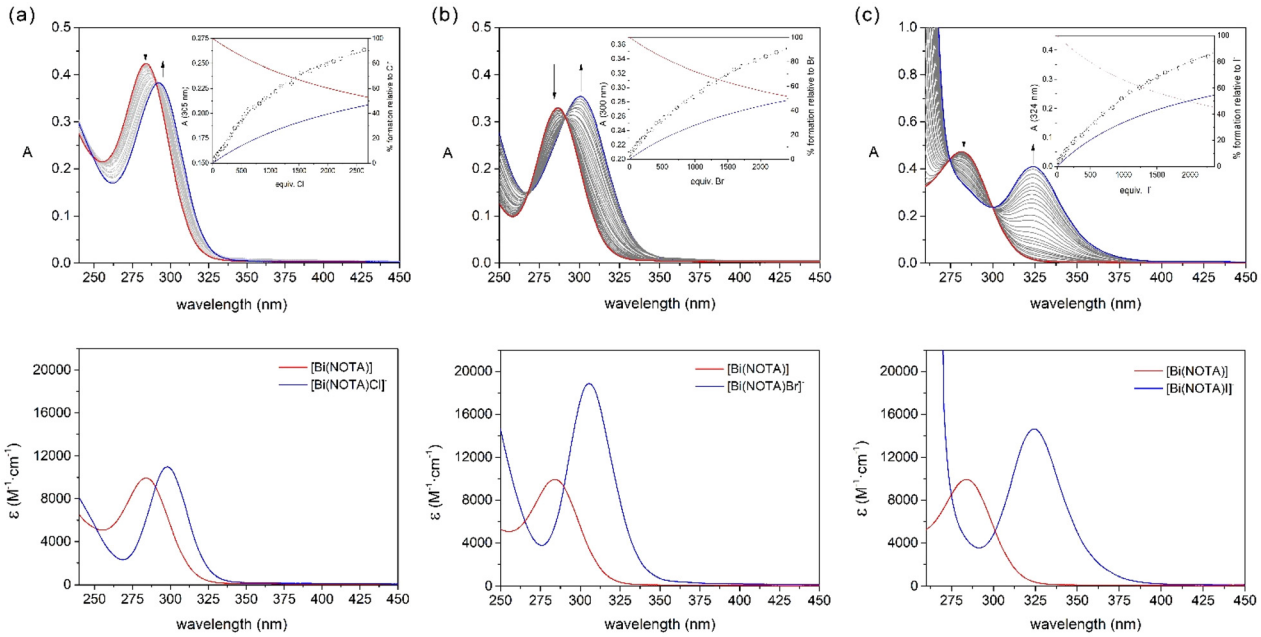

Fig. 3 Absorption spectra recorded during the course of the titrations of [Bi(NOTA)] (5×10^{-5} M) with (a) KCl, (b) KBr and (c) KI. The insets in the upper panels show the titration profiles at selected wavelengths and the lower panels present comparisons of the spectra calculated for the [Bi(NOTA)X]$^{-}$ species and that of [Bi(NOTA)].

Table 4 Bond distances (Å) of the Bi(III) coordination environment obtained with DFT and composition of the $6s^2$ lone pair of Bi(III) obtained NBO analysis.[a]

	Bi–O	Bi–N	Bi–X	NBO
[Bi(NOTA)]	2.378(4)	2.481(1)	—	s(96.87%)p(3.11%)
[Bi(NOTA)Cl]$^{-}$	2.386(2)	2.610(2)	2.822	s(99.60%)p(0.39%)
[Bi(NOTA)Br]$^{-}$	2.366(7)	2.685(2)	2.995	s(99.91%)p(0.07%)
[Bi(NOTA)I]$^{-}$	2.367(12)	2.656(1)	3.311	s(99.74%)p(0.24%)

[a] Mean values are provided for bond distances with standard deviation within parentheses.

dinating with the metal ion. Thus, all subsequent calculations were performed on the [Bi(NOTA)] system.

The optimized geometries of the [Bi(NOTA)X]$^{-}$ systems indicate that anion binding provokes an important elongation of the Bi–N bonds, while the Bi–O bonds experience minor changes upon halide coordination (Table 4). The calculated Bi–O and Bi–N distances are within the range observed for seven-coordinate complexes with polyaminocarboxylate ligands.[1] The Bi–X distances are within the rather broad range observed for $[BiX_6]^{3-}$,[44,45] $[Bi_2X_{10}]^{4-}$,[46] $[Bi_3X_{12}]^{3-}$[47] and $[\{BiX_4\}_n]^{-}$[19,48] entities (Bi–Cl = 2.55–2.91 Å; Bi–Br = 2.68–3.18 Å; Bi–I = 2.90–3.37 Å). A ternary complex of [Bi(EDTA)]$^{-}$ with chloride displays a Bi–Cl distance of 2.922 Å in the solid state.[1] In the latter structure, the metal ion is eight-coordinated, with the coordination sphere being completed by a bridging carboxylate group.

The analysis of the natural bond orbitals (NBOs) in [Bi(NOTA)] (Table 4) indicates that the $6s^2$ lone pair of Bi(III) is polarised by a significant 6p contribution (3.11%), which signals a stereochemically active lone pair and thus a hemidirected structure. This type of structure is characterized by a void in the coordination sphere along the direction to which the stereochemically active lone pair is directed, along with a shortening of the bond distances in the opposite direction. This situation parallels what was found previously for Pb(II) complexes.[15,49] The studies reported before showed 6p contributions <2.53% for a rather broad series of Bi(III) complexes,[12,16,50] which indicates that the lone pair is stereochemically active in [Bi(NOTA)]. Inspection of the NBOs shows that the $6s^2$ lone pair in [Bi(NOTA)] is indeed directed along the C_3 symmetry axis of the molecule in a direction opposite to the macrocyclic unit, just on the side where a void in the coordination sphere is observed (Fig. 4). As a result, the Bi–N bonds, which are situated opposite with respect to the lone pair, are rather short. Anion coordination takes place at the C_3 axis in the direction where the Bi(III) $6s^2$ lone pair is placed. Thus, anion coordination fills the void in the coordination sphere resulting from the stereochemical activity of the lone pair, resulting in a decreased polarisation of the lone pair with 6p contribution and holodirected structures. This is confirmed by the rather spherical distribution of donor atoms around the Bi(III) ion in Fig. 4b. We note that the 6p contribution to the Bi(III) $6s^2$ lone pair correlates well with the calculated Bi–N distances.

QD-NEVPT2 calculations on the [Bi(NOTA)] and [Bi(NOTA)X]$^{-}$ (X = Cl, Br or I) systems

We initiated our QD-NEVPT2 calculations using a CAS(2,4) active space. As observed for the chloride complexes, these calculations provided up to five virtual orbitals with significant Bi

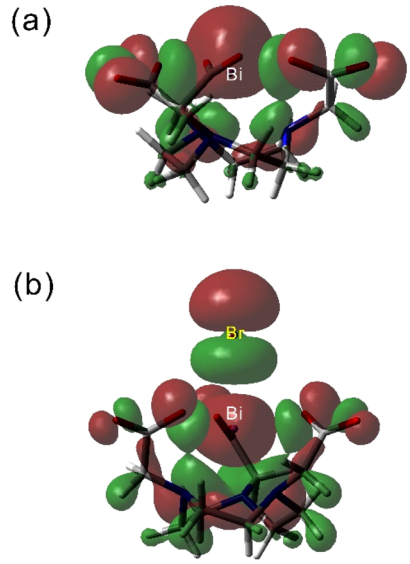

Fig. 4 Views of the isodensity surfaces (0.02 a. u.) of the HOMOs obtained with DFT for [Bi(NOTA)] (a) and [Bi(NOTA)Br]$^-$ (b).

6s/6p character, and thus the active space was enlarged. Our QD-NEVPT2 calculations based on CAS(2,9) wave functions predict the energy of the main absorption band observed in the experimental spectra with a rather good accuracy (Table 5). For C_3 symmetry, the $^3P_1$ level splits into two states, and thus the $^3P_1 \leftarrow {}^1S_0$ absorption contains two contributions from $^3E \leftarrow {}^1A$ and $^3A \leftarrow {}^1A$ excitation, both characterized by relatively high oscillator strengths. As observed for $[BiCl_5]^{2-}$, the reduced symmetry allows for some mixing of the $^3E(^3P_2)$ and $^3E(^3P_1)$ states, resulting in calculated f_{osc} values in the range of 17 to 79 for the $^3E(^3P_2) \leftarrow {}^1A$ excitation. However, these transitions, as well as those involving levels arising from the $^1P_1$ free-ion term, occur at high energies (λ < 260 nm) and could not be observed in the experimental absorption spectra.

Our calculations predict a shift of the absorption band to lower energies arising from $^3E(^3P_1) \leftarrow {}^1A$ and $^3A(^3P_1) \leftarrow {}^1A$ excitation upon halide binding, an effect that is enhanced when following the sequence $Cl^- < Br^- < I^-$. This is in good agreement with the experimental evidence. The energies of the spin–orbit free states ^3P and ^1P decrease significantly following this trend (Table 3), which suggests that the shift of the absorption $^3P_1 \leftarrow {}^1S_0$ is related to an increased covalent character of the Bi–ligand (s) bonds. Furthermore, the values of the SOC constants λ estimated with the methodology outlined above are all very similar, with a somewhat higher value being estimated for [Bi(NOTA)Cl]$^-$ (Table 3). Additional support for the role of covalency in the position of the $^3P_1 \leftarrow {}^1S_0$ absorption band is provided by the plot of the energies calculated for the spin–orbit free ^3P state and the position of the $^3P_1 \leftarrow {}^1S_0$ predicted by QD-NEVPT2 calculations (Fig. 5). Our results evidence a very good linear correlation (R^2 > 0.996), which supports our hypothesis.

Recent studies evidenced that the position of 6sp ← 6s in Pb(II) complexes with ligands containing N,O donor sets shifted to longer wavelengths as the number of N atoms of the ligand increased.[20] The position of the absorption maxima observed for [Bi(NOTA)] (282 nm, N_3O_3 donor set), [Bi(DO3A)] (299 nm, N_4O_3 donor set)[16] and [Bi(Me$_2$DODPA)]$^+$ (350 nm, N_6O_2 donor set)[51] follow this trend, which is likely related to a more important covalent character of the Bi–N bonds compared with the Bi–O counterparts. Hancock *et al.* tentatively suggested that the transition is observed at longer wavelengths for complexes where the Pb(II) environment is holodirected compared to

Table 5 Wavelengths (nm), energies (cm^{-1}) of the levels arising from the 6s^{1}6p^1 configuration of [Bi(NOTA)] and [Bi(NOTA)X]$^{\bullet-}$ complexes (X = Cl, Br or I) with respect to the ground $^1S_0$ level and oscillator strengths (f_{osc}).[a]

[Bi(NOTA)]		$^3P_0$ (^3A)	$^3P_1$ ($^3E + {}^3A$)	$^3P_2$ ($^3A + {}^3E + {}^3E$)	$^1P_1$ ($^1A + {}^1E$)
	λ (nm)	274.2	270.0(×2); 265.7	217.3; 215.2(×2); 204.6(×2)	208.6; 197.8(×2)
	λ_{exp} [a] (nm)	—	282	—	
	Energy (cm^{-1})	36 467	37 037; 37 355	46 009; 46 472; 48 881	47 936; 50 552
	$10^3 \times f_{osc}$	0.0	133.7; 118.6	0.0; 79.1; 0.6	322.6; 675.2
	ε [a]/M^{-1} cm^{-1}	—	9900	—	
[Bi(NOTA)Cl]$^-$	λ (nm)	393.4	289.0(×2); 281.6	217.3(×2); 215(×2); 212.9	211.1(×2); 198.9
	λ_{exp} [a] (nm)		298		
	Energy (cm^{-1})	34 083	34 605; 35 509	46 030; 46 542; 46 976	47 375; 50 266
	$10^3 \times f_{osc}$	0.0	31.6; 9.9	0.0; 25.4; 0.0	63.7; 130.1
	ε [a]/M^{-1} cm^{-1}		11 000		
[Bi(NOTA)Br]$^-$	λ (nm)	299.7	301.8; 296.8(×2)	225.6(×2); 224.4(×2); 223.6	222.4(×2); 220.8
	λ_{exp} [a] (nm)		305		
	Energy (cm^{-1})	33 364	33 134; 33 697	44 336; 44 568; 44 732	44 971; 45 295
	$10^3 \times f_{osc}$	0.0	25.2; 66.5	0.5; 16.9	235.7; 8.8
	ε [a]/M^{-1} cm^{-1}		18 900		
[Bi(NOTA)I]$^-$	λ (nm)	361.5	359.1(×2); 333.2	260.0; 259.2(×2); 252.8(×2)	250.1(×2); 235.9
	λ_{exp} [a] (nm)		325		
	Energy (cm^{-1})	27 660	27 848; 30 016	38 465; 38 572; 39 562	39 989; 42 397
	$10^3 \times f_{osc}$	0.0	44.1; 8.4	0.0; 26.9; 0.1	183.9; 92.1
	ε [a]/M^{-1} cm^{-1}		14 600		

[a] Average values are provided for nearly degenerate levels, with their number indicated within parentheses. All calculations are performed using CAS(2,9) wave functions.

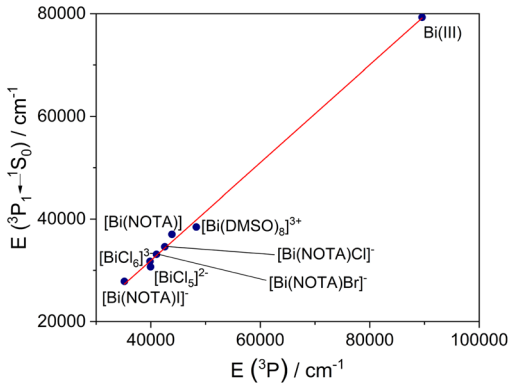

Fig. 5 Correlation between the energies predicted for the spin–orbit free ^3P state and the calculated position of the $^3P_1 \leftarrow {}^1S_0$ transition.

where it is hemidirected.[20] Further studies are certainly required to confirm this hypothesis. However, we note that hemidirected structures are favoured by the presence of hard donor atoms and low coordination numbers.[15,49] Thus, the observation made by Hancock on Pb(II) complexes appears to be consistent with the results obtained here, as holodirected structures are expected to have more covalent metal–ligand interactions.

Conclusions

We conducted an experimental and theoretical study to understand the factors that affect the 6sp ← 6s spectra of Bi(III) complexes. An important outcome of this study is the deficiencies of common density functionals in predicting the energies of the excited states of the free Bi(III) ion. However, QD-NEVPT2 performed very well both for the free Bi(III) ion and different Bi(III) complexes, particularly using a CAS(2,9) active space. Our calculations performed on the $[BiCl_6]^{3-}$ and $[BiCl_5]^{2-}$ systems revealed the effects that decreasing complex symmetry has on the absorption spectra. A comparison of the absorption spectra of these complexes with that of $[Bi(DMSO)]^{3+}$, in which harder DMSO ligands are coordinated through the O atom, suggested that the covalence of the metal–ligand bonds has an important impact on the position of the $^3P_1 \leftarrow {}^1S_0$ absorption band, while differences in SOC appear to have a minor effect. This was confirmed by the analysis of the absorption spectra of the [Bi(NOTA)] and $[Bi(NOTA)X]^-$ complexes. We envisage that the results reported here will help infer detailed structural information from the absorption spectra of Bi(III) complexes, thereby aiding the characterization of Bi(III) complexes for different applications, including targeted alpha therapy.

Experimental and computational section

General

NOTA was purchased from Chematech (Dijon, France). All other solvents and reagents used were purchased from commercial sources, had reagent grade quality and were used as supplied. NMR spectra were recorded using a Bruker Avance 400 spectrometer at 25 °C. Elemental analyses were conducted on a Thermo Finnigan Flash EA 1112 instrument. Mass spectra were obtained with an LTQ-Orbitrap Discovery mass spectrometer in ESI positive mode. Purifications were carried out on a medium performance liquid chromatography (MPLC) Puriflash XS 420 InterChim Chromatographer equipped with a UV-DAD detector and a 20 g BGB Aquarius C18AQ reverse phase column (100 Å, spherical, 15 µm). Aqueous solutions were lyophilized in a Biobase BK-FD10 Series Vacuum Freeze Dryer.

Preparation of [Bi(NOTA)]

NOTA (25.7 mg, 0.0847 mmol) was suspended in EtOH and heated to 80 °C. $Bi(NO_3)_3{\cdot}5H_2O$ (44.3 mg, 0.0913 mmol) was then added and the mixture was refluxed for 2 hours. After solvent evaporation, the crude was dissolved in 0.5 mL of H_2O and the pH was adjusted to around 7 with a diluted NaOH solution for the complex to dissolve. This solution was injected into an MPLC and purified by reverse phase using water as a mobile phase (compound eluted at 1.26 CV, 1 : 44 min : s, with salts eluting at the solvent front at 0.83 CV, 1 : 09 min : s). The fraction containing the compound of interest was lyophilized, affording a white solid (33.7 mg, 65% yield). ^{1}H-NMR (400 MHz, D_2O): δ (ppm) 4.33 (s, 6H), 3.95–3.80 (m, 6H), 3.68–3.53 (m, 6H).^{13}C{^{1}H}-NMR (75 MHz, D_2O): δ 177.71, 63.37, 55.84. Elem. anal. found: C 23,59%; H 3,36%; N 9,07%. Calc. for $[C_{12}H_{18}BiN_3O_6](NaNO_3)(H_2O)$: C 23,54%; H 3,29%; N 9,15%. MS (ESI$^+$, %BPI): *m*/*z* 510.1072 (35), 535.0891 (100), 786.6393 (23), 1041.1903 (61), 1550.2897 (24). Calc. for $[C_{12}H_{19}BiN_3O_6]^+$: 510.1072; $[C_{12}H_{18}BiN_3O_6Na]^+$: 532.0892; $[(C_{12}H_{18}BiN_3O_6)_2(C_{12}H_{19}BiN_3O_6)Na]^{2+}$: 775.9482, $[(C_{12}H_{18}BiN_3O_6)_2Na]^+$: 1041.1891, $[(C_{12}H_{18}BiN_3O_6)_3Na]^+$: 1550.2891.

Absorption spectra

Spectroscopic measurements were performed with 4 mm path length quartz suprasil certified cells (Helma Analytics) using a double-beam JENWAY 6850 UV-vis spectrophotometer. The DMSO solvate was prepared by dissolving $Bi(NO_3)_3{\cdot}5H_2O$ in DMSO while the $[BiCl_5]^{2-}$ complex was prepared by dissolving $BiCl_3$ in a 2 M HCl solution to obtain a 5×10^{-5} M concentration of the complex. The $[BiCl_6]^{3-}$ complex was prepared by dissolving $BiCl_3$ in acetonitrile and adding 45 equiv. of $(^nBu)_4NCl$ (final concentration of the complex (5×10^{-5} M)).

Spectroscopic titrations were performed with 1 cm path length quartz suprasil certified cells (Helma Analytics). Anion binding studies were carried out by using 5×10^{-5} M solutions of [Bi(NOTA)] buffered at pH 7 using MOPS, by adding aliquots of a solution containing the corresponding halide (0.25 M prepared from the potassium salt) and 5×10^{-5} M [Bi(NOTA)], to avoid dilution. The UV-vis spectra were recorded after each aliquot addition and the spectrophotometric data were analysed using HYPERQUAD.[52]

Computational details

The geometries of the Bi(III) complexes were optimized using Gaussian 16,[53] employing the range-separated hybrid wB97XD functional,[54] which incorporates empirical dispersion corrections. Relativistic effects were incorporated using the relativistic effective core potential ECP60MDF for Bi, which includes 60 electrons in the core,[55] together with the associated cc-pVTZ (12s11p8d1f)/[5s4p3d1f] basis set.[56] For I, we selected the relativistic effective core potential ECP28MDF and the associated cc-pVTZ-PP (27s24p11d1f)/[5s4p3d1f] basis set.[57] The standard Def2-TZVPP basis set was selected for all other atoms.[58] The structure of the $[Bi(DMSO)_8]^{3+}$ complex was optimized in the gas phase, as the incorporation of solvent effects with a polarized continuum model (PCM) prevented convergence. For all other systems, solvent effects were the integral equation formalism variant of PCM (IEF-PCM variant).[59,60] Frequency calculations confirmed that the optimized geometries corresponded to actual energy minima. The size of the integration grid was set with the integral = ultrafine keyword. Natural bond orbital analysis was performed with the NBO program (version 3.1)[61] available in Gaussian.

Complete active space self-consistent field (CASSCF)[62] calculations were performed with the ORCA program package (version 5.0.3).[63,64] Relativistic effects were taken into account with the Douglas–Kroll–Hess (DKH2) method,[65,66] using a finite nucleus model.[67] The active space included the $6s^2$ electrons of Bi(III) distributed over four [CAS(2,4)] or nine [CAS(2,9)] frontier orbitals with 6s and 6p character. The state average CASSCF calculation included 6 triplet and 10 singlet roots. Dynamic correlation effects were considered using the strongly contracted implementation of N-electron valence state perturbation theory (SC-NEVPT2),[68–70] employing the quasi-degenerate (QD-NEVPT2) variant,[71,72] unless otherwise stated. NEVPT2 calculations employed the frozen core approximation using the default ORCA settings (see Table S9, ESI,† for details). In these calculations, we used the SARC-DKH-TZVPP[73] basis set for Bi and the DKH-def2-TZVPP basis set for ligand atoms, which uses the exponents of the def2-TZVPP[58] basis set and was recontracted by D. A. Pantazis for DKH2 calculations. The resolution of identity and chain of spheres (RIJCOSX)[74,75] method was used to accelerate the calculations with auxiliary basis sets generated by ORCA with the AutoAux[76] procedure. SOC effects were incorporated using quasi-degenerate perturbation theory (QDPT).[77,78] Solvent effects were included using the SMD solvation model.[79] TDDFT calculations were performed with ORCA, using the DKH method with the SARC-DKH-TZVPP[73] basis set for Bi(III) and the PBE,[80] PBE0[81] and TPSS[82] functionals. Spin–orbit coupling was considered using the spin–orbit mean-field (SOMF(1X)) method.[83,84]

Author contributions

C. P.-I conceived and supervised the project. Theoretical calculations were performed by F. L.-M., C. H., A. R.-R., and C. P.-I. Synthesis of the complexes was carried out by C. H. Spectroscopic measurements were recorded by C. H. and analysed by D. E.-G. The manuscript was written through the contributions of all authors. All the authors gave their approval for manuscript submission.

Conflicts of interest

There are no conflicts to declare.

Acknowledgements

Authors D. E.-G. and C. P.-I. thank Ministerio de Ciencia e Innovación (Grants PID2019-104626GB-I00 and PID2022-138335NB-I00) and Xunta de Galicia (ED431C 2023/33) for generous financial support. C. H. thanks Ministerio de Ciencia e Innovación (Grant PRE2020-092888) for funding her PhD contract. A. R.-R. acknowledges Ministerio de Ciencia e Innovación for generous financial support (PID2019-108352RJ-I00). The authors thank Centro de Supercomputación de Galicia (CESGA) for providing the supercomputing facilities. Funding for open access provided by Universidade da Coruña/CISUG.

References

1 V. Stavila, R. L. Davidovich, A. Gulea and K. H. Whitmire, *Coord. Chem. Rev.*, 2006, **250**, 2782–2810.
2 G. G. Briand and N. Burford, *Chem. Rev.*, 1999, **99**, 2601–2658.
3 R. Eychenne, M. Chérel, F. Haddad, F. Guérard and J.-F. Gestin, *Pharmaceutics*, 2021, **13**, 906.
4 S. Hassfjell and M. W. Brechbiel, *Chem. Rev.*, 2001, **101**, 2019–2036.
5 M. W. Brechbiel, *Dalton Trans.*, 2007, 4918.
6 G. Montavon, A. Le Du, J. Champion, T. Rabung and A. Morgenstern, *Dalton Trans.*, 2012, **41**, 8615.
7 D. Horváth, A. Vágner, D. Szikra, G. Trencsényi, N. Demitri, N. Guidolin, A. Maiocchi, S. Ghiani, F. Travagin, G. B. Giovenzana and Z. Baranyai, *Angew. Chem., Int. Ed.*, 2022, **61**, e202207120.
8 E. V. Matazova, B. V. Egorova, E. A. Konopkina, G. Y. Aleshin, A. D. Zubenko, A. A. Mitrofanov, K. V. Karpov, O. A. Fedorova, Y. V. Fedorov and S. N. Kalmykov, *MedChemComm*, 2019, **10**, 1641–1645.
9 J. J. Wilson, M. Ferrier, V. Radchenko, J. R. Maassen, J. W. Engle, E. R. Batista, R. L. Martin, F. M. Nortier, M. E. Fassbender, K. D. John and E. R. Birnbaum, *Nucl. Med. Biol.*, 2015, **42**, 428–438.
10 D. Horváth, F. Travagin, N. Guidolin, F. Buonsanti, G. Tircsó, I. Tóth, F. Bruchertseifer, A. Morgenstern, J. Notni, G. B. Giovenzana and Z. Baranyai, *Inorg. Chem. Front.*, 2021, **8**, 3893–3904.

11 F. Lucio-Martínez, D. Esteban-Gómez, L. Valencia, D. Horváth, D. Szücs, A. Fekete, D. Szikra, G. Tircsó and C. Platas-Iglesias, *Chem. Commun.*, 2023, **59**, 3443–3446.
12 D. J. Fiszbein, V. Brown, N. A. Thiele, J. J. Woods, L. Wharton, S. N. MacMillan, V. Radchenko, C. F. Ramogida and J. J. Wilson, *Inorg. Chem.*, 2021, **60**, 9199–9211.
13 H. A. Song, C. S. Kang, K. E. Baidoo, D. E. Milenic, Y. Chen, A. Dai, M. W. Brechbiel and H.-S. Chong, *Bioconjugate Chem.*, 2011, **22**, 1128–1135.
14 A. Hu, V. Brown, S. N. MacMillan, V. Radchenko, H. Yang, L. Wharton, C. F. Ramogida and J. J. Wilson, *Inorg. Chem.*, 2022, **61**, 801–806.
15 L. Shimoni-Livny, J. P. Glusker and C. W. Bock, *Inorg. Chem.*, 1998, **37**, 1853–1867.
16 R. Pujales-Paradela, A. Rodríguez-Rodríguez, A. Gayoso-Padula, I. Brandariz, L. Valencia, D. Esteban-Gómez and C. Platas-Iglesias, *Dalton Trans.*, 2018, **47**, 13830–13842.
17 R. Luckay, I. Cukrowski, J. Mashishi, J. H. Reibenspies, A. H. Bond, R. D. Rogers and R. D. Hancock, *J. Chem. Soc., Dalton Trans.*, 1997, 901–908.
18 A. K. Adcock, R. J. Batrice, J. A. Bertke and K. E. Knope, *Eur. J. Inorg. Chem.*, 2017, 1435–1445.
19 R. D. Rogers, A. H. Bond, S. Aguinaga and A. Reyes, *J. Am. Chem. Soc.*, 1992, **114**, 2967–2977.
20 J. W. Nugent, H.-S. Lee, J. H. Reibenspies and R. D. Hancock, *Polyhedron*, 2015, **91**, 120–127.
21 W. R. Mason, *Inorg. Chem.*, 1999, **38**, 2742–2745.
22 C. Liao, J. M. Kasper, A. J. Jenkins, P. Yang, E. R. Batista, M. J. Frisch and X. Li, *JACS Au*, 2023, **3**, 358–367.
23 J. Näslund, I. Persson and M. Sandström, *Inorg. Chem.*, 2000, **39**, 4012–4021.
24 K. Kumar, M. Magerstadt and O. A. Gansow, *J. Chem. Soc., Chem. Commun.*, 1989, 145–146.
25 C. S. Kang, H. A. Song, D. E. Milenic, K. E. Baidoo, M. W. Brechbiel and H.-S. Chong, *Nucl. Med. Biol.*, 2013, **40**, 600–605.
26 H.-S. Chong, X. Ma, T. Le, B. Kwamena, D. E. Milenic, E. D. Brady, H. A. Song and M. W. Brechbiel, *J. Med. Chem.*, 2008, **51**, 118–125.
27 G. Boulon, *J. Phys.*, 1971, **32**, 333–347.
28 F. Réal, V. Vallet, J.-P. Flament and J. Schamps, *J. Chem. Phys.*, 2006, **125**, 174709.
29 K. Oldenburg and A. Vogler, *Z. fur Naturforsch. – B*, 1993, **48**, 1519–1523.
30 H. Nikol and A. Vogler, *J. Am. Chem. Soc.*, 1991, **113**, 8988–8990.
31 B. E. Etschmann, W. Liu, A. Pring, P. V. Grundler, B. Tooth, S. Borg, D. Testemale, D. Brewe and J. Brugger, *Chem. Geol.*, 2016, **425**, 37–51.
32 L. Newman and D. N. Hume, *J. Am. Chem. Soc.*, 1957, **79**, 4576–4581.
33 A. Stoïanov, J. Champion and R. Maurice, *Inorg. Chem.*, 2019, **58**, 7036–7043.
34 N. Zhutova, F. Réal, E. Renault, V. Vallet and R. Maurice, *Phys. Chem. Chem. Phys.*, 2023, **25**, 24603–24612.
35 P.-O. Löwdin, *J. Chem. Phys.*, 1950, **18**, 365–375.
36 L. Freitag, S. Knecht, S. F. Keller, M. G. Delcey, F. Aquilante, T. B. Pedersen, R. Lindh, M. Reiher and L. González, *Phys. Chem. Chem. Phys.*, 2015, **17**, 14383–14392.
37 S. K. Singh, M. Atanasov and F. Neese, *J. Chem. Theory Comput.*, 2018, **14**, 4662–4677.
38 K. Andersson and B. O. Roos, *Chem. Phys. Lett.*, 1992, **191**, 507–514.
39 S. Ahrland and I. Grenthe, *Acta Chem. Scand.*, 1957, **11**, 1111–1130.
40 E. J. Corey and J. C. Bailar, *J. Am. Chem. Soc.*, 1959, **81**, 2620–2629.
41 J. K. Beattie, *Acc. Chem. Res.*, 1971, **4**, 253–259.
42 C. J. Broan, J. P. L. Cox, A. S. Craig, R. Kataky, D. Parker, A. Harrison, A. M. Randall and G. Ferguson, *J. Chem. Soc., Perkin Trans. 2*, 1991, 87–99.
43 P. R. W. J. Davey, C. M. Forsyth and B. M. Paterson, *ChemistrySelect*, 2022, **7**, e202103698.
44 L. P. Battaglia, A. B. Corradi, G. Pelizzi and M. E. Vidoni, *J. Chem. Soc., Dalton Trans.*, 1977, 1141–1144.
45 M. Li and R. K. Li, *CrystEngComm*, 2013, **15**, 4176.
46 A. García-Fernández, I. Marcos-Cives, C. Platas-Iglesias, S. Castro-García, D. Vázquez-García, A. Fernández and M. Sánchez-Andújar, *Inorg. Chem.*, 2018, **57**, 7655–7664.
47 C. J. Carmalt, L. J. Farrugia and N. C. Norman, *Z. Anorg. Allg. Chem.*, 1995, **621**, 47–56.
48 U. Geiser, H. H. Wang, S. M. Budz, M. J. Lowry, J. M. Williams, J. Ren and M. H. Whangbo, *Inorg. Chem.*, 1990, **29**, 1611–1614.
49 D. Esteban-Gómez, C. Platas-Iglesias, T. Enríquez-Pérez, F. Avecilla, A. De Blas and T. Rodríguez-Blas, *Inorg. Chem.*, 2006, **45**, 5407–5416.
50 A. Ingham, L. Wharton, T. El Sayed, L. Southcott, B. L. McNeil, M. B. Ezhova, B. O. Patrick, M. D. G. Jaraquemada-Peláez and C. Orvig, *Inorg. Chem.*, 2022, **61**, 9119–9137.
51 L. M. P. Lima, M. Beyler, R. Delgado, C. Platas-Iglesias and R. Tripier, *Inorg. Chem.*, 2015, **54**, 7045–7057.
52 P. Gans, A. Sabatini and A. Vacca, *Talanta*, 1996, **43**, 1739–1753.
53 M. J. Frisch, G. W. Trucks, H. B. Schlegel, G. E. Scuseria, M. A. Robb, J. R. Cheeseman, G. Scalmani, V. Barone, G. A. Petersson, H. Nakatsuji, X. Li, M. Caricato, A. V. Marenich, J. Bloino, B. G. Janesko, R. Gomperts, B. Mennucci, H. P. Hratchian, J. V. Ortiz, A. F. Izmaylov, J. L. Sonnenberg, W. F. Ding, F. Lipparini, F. Egidi, J. Goings, B. Peng, A. Petrone, T. Henderson, D. Ranasinghe, V. G. Zakrzewski, J. Gao, N. Rega, G. Zheng, W. Liang, M. Hada, M. Ehara, K. Toyota, R. Fukuda, J. Hasegawa, M. Ishida, T. Nakajima, Y. Honda, O. Kitao, H. Nakai, T. Vreven, K. Throssell, J. A. Montgomery Jr., J. E. Peralta, F. Ogliaro, M. J. Bearpark, J. J. Heyd, E. N. Brothers, K. N. Kudin, V. N. Staroverov, T. A. Keith, R. Kobayashi, J. Normand, K. Raghavachari, A. P. Rendell, J. C. Burant, S. S. Iyengar, J. Tomasi, M. Cossi,

J. M. Millam, M. Klene, C. Adamo, R. Cammi, J. W. Ochterski, R. L. Martin, K. Morokuma, O. Farkas, J. B. Foresman and D. J. Fox, *Gaussian 16 Rev. C.01*, 2016.
54 J.-D. Chai and M. Head-Gordon, *J. Chem. Phys.*, 2008, **128**, 084106.
55 B. Metz, H. Stoll and M. Dolg, *J. Chem. Phys.*, 2000, **113**, 2563–2569.
56 K. A. Peterson, *J. Chem. Phys.*, 2003, **119**, 11099–11112.
57 K. A. Peterson, B. C. Shepler, D. Figgen and H. Stoll, *J. Phys. Chem. A*, 2006, **110**, 13877–13883.
58 F. Weigend and R. Ahlrichs, *Phys. Chem. Chem. Phys.*, 2005, **7**, 3297–3305.
59 J. Tomasi, B. Mennucci and E. Cancès, *J. Mol. Struct.: THEOCHEM*, 1999, **464**, 211–226.
60 J. Tomasi, B. Mennucci and R. Cammi, *Chem. Rev.*, 2005, **105**, 2999–3094.
61 E. D. Glendening, A. E. Reed, J. E. Carpenter and F. Weinhold, *NBO (version 3.1)*, Gaussian Inc., Pittsburgh, 2003.
62 P.-Å. Malmqvist and B. O. Roos, *Chem. Phys. Lett.*, 1989, **155**, 189–194.
63 F. Neese, *Wiley Interdiscip. Rev.: Comput. Mol. Sci.*, 2012, **2**, 73–78.
64 F. Neese, *Wiley Interdiscip. Rev.: Comput. Mol. Sci.*, 2018, **8**, e1327.
65 M. Reiher, *Theor. Chem. Acc.*, 2006, **116**, 241–252.
66 M. Barysz and A. J. Sadlej, *J. Mol. Struct.: THEOCHEM*, 2001, **573**, 181–200.
67 L. Visscher and K. G. Dyall, *At. Data Nucl. Data Tables*, 1997, **67**, 207–224.
68 C. Angeli, R. Cimiraglia, S. Evangelisti, T. Leininger and J.-P. Malrieu, *J. Chem. Phys.*, 2001, **114**, 10252–10264.
69 C. Angeli, R. Cimiraglia and J.-P. Malrieu, *Chem. Phys. Lett.*, 2001, **350**, 297–305.
70 C. Angeli, R. Cimiraglia and J.-P. Malrieu, *J. Chem. Phys.*, 2002, **117**, 9138–9153.
71 C. Angeli, S. Borini, M. Cestari and R. Cimiraglia, *J. Chem. Phys.*, 2004, **121**, 4043–4049.
72 L. Lang, K. Sivalingam and F. Neese, *J. Chem. Phys.*, 2020, **152**, 014109.
73 D. A. Pantazis and F. Neese, *Theor. Chem. Acc.*, 2012, **131**, 1292.
74 F. Neese, *J. Comput. Chem.*, 2003, **24**, 1740–1747.
75 R. Izsák and F. Neese, *J. Chem. Phys.*, 2011, **135**, 144105.
76 G. L. Stoychev, A. A. Auer and F. Neese, *J. Chem. Theory Comput.*, 2017, **13**, 554–562.
77 D. Maganas, S. Sottini, P. Kyritsis, E. J. J. Groenen and F. Neese, *Inorg. Chem.*, 2011, **50**, 8741–8754.
78 M. Atanasov, D. Aravena, E. Suturina, E. Bill, D. Maganas and F. Neese, *Coord. Chem. Rev.*, 2015, **289–290**, 177–214.
79 A. V. Marenich, C. J. Cramer and D. G. Truhlar, *J. Phys. Chem. B*, 2009, **113**, 6378–6396.
80 J. P. Perdew, K. Burke and M. Ernzerhof, *Phys. Rev. Lett.*, 1996, **77**, 3865–3868.
81 C. Adamo and V. Barone, *J. Chem. Phys.*, 1999, **110**, 6158–6170.
82 J. Tao, J. P. Perdew, V. N. Staroverov and G. E. Scuseria, *Phys. Rev. Lett.*, 2003, **91**, 146401.
83 F. Neese, *J. Chem. Phys.*, 2005, **122**, 034107.
84 B. A. Heß, C. M. Marian, U. Wahlgren and O. Gropen, *Chem. Phys. Lett.*, 1996, **251**, 365–371.